A Finite-Difference Time-Domain Method for Solving Electromagnetic Problems with Bandpass-Limited Sources

J. D. Pursel, *Member, IEEE,* and P. M. Goggans, *Member, IEEE*

***Abstract*— The complex-envelope representation of bandpass-limited signals is used to formulate a bandpass-limited vector wave equation and a new finite-difference time-domain (FDTD) scheme that solves the bandpass-limited vector wave equation is presented. For narrow-band electromagnetic systems, this new method allows the time step to be several orders of magnitude larger than current FDTD formulations while maintaining an amplification factor equal to one. Example results obtained by this method are presented and compared with analytic solutions.**

***Index Terms*— Bandpass-limited, complex-envelope, FDTD, wave equation.**

I. Introduction

THE usual finite-difference time-domain (FDTD) solution of the electromagnetic wave equation uses time and spatial sampling according to the lowpass-limited (LPL) sampling theorem. For time sampling this means that the time step must be set in accordance with maximum frequency in the source signal. However, for radar and communication systems problems the source signal is usually bandpass-limited (BPL) rather than lowpass-limited. The bandpass-limited sampling theorem states that using the proper techniques, the signal can be sampled in accordance with the bandwidth of the signal source rather than its maximum frequency. This suggests that the FDTD method can be modified so that the required time step for BPL signals is significantly increased compared to the conventional FDTD method.

One way of modifying the FDTD method is to use the complex envelope representation of BPL signals [1], [2]. The complex envelope representation of a real BPL signal yields a complex LPL signal with a maximum frequency equal to one half the bandwidth of the original signal.

II. Complex-Envelope Representation

A real bandpass-limited signal source $v(t)$ can be expressed in the form [1], [3]

$$v(t) = v_p(t)\cos(2\pi f_0 t) - v_q(t)\sin(2\pi f_0 t) \tag{1}$$

where $v_p(t)$ and $v_q(t)$ are the in-phase and quadrature portions of $v(t)$ and f_0 is the center frequency of $v(t)$ [1]. The bandwidth B and center frequency of $v(t)$ can be expressed in terms of $f_{\max}$, the maximum frequency in $v(t)$, and $f_{\min}$, the minimum frequency in $v(t)$. For $f_{\max} > f_{\min} > 0$, the relationships are

$$B = f_{\max} - f_{\min} \tag{2}$$

and

$$f_0 = \frac{f_{\max} + f_{\min}}{2}. \tag{3}$$

The time functions $v_p(t)$ and $v_q(t)$ are real and low-pass limited with bandwidth $B/2$.

Haykin [1] introduces the complex envelope notation to make the bandpass-limited signal and system problem isomorphic to the base-band (LPL) signal and system problem. The complex envelope of $v(t)$ is denoted as $\tilde{v}(t)$ and is defined by

$$\tilde{v}(t) = v_p(t) + jv_q(t) \tag{4}$$

where the function $v(t)$ can be recovered from $\tilde{v}(t)$ using the expression

$$v(t) = \Re\{\tilde{v}(t)\,\exp(j2\pi f_0 t)\}. \tag{5}$$

The Fourier transform of the complex envelope can be determined from the Fourier transform of $v(t)$ using

$$\tilde{V}(f) = V(f + f_0) + \mathrm{sgn}(f + f_0)V(f + f_0) \tag{6}$$

where

$$\mathrm{sgn}(f) = \begin{cases} 1, & \text{for } f > 0 \\ 0, & \text{for } f = 0 \\ -1, & \text{for } f < 0. \end{cases} \tag{7}$$

Here, the standard engineering definition of the Fourier transform is used so that

$$V(f) = \int_{-\infty}^{\infty} v(t)e^{-j2\pi ft}\,dt \tag{8}$$

and

$$v(t) = \int_{-\infty}^{\infty} V(f)e^{+j2\pi ft}\,df. \tag{9}$$

Manuscript received August 25, 1997; revised June 8, 1998.

J. D. Pursel was with the Department of Electrical Engineering, University of Mississippi, University, MS 38677 USA. He is now with the Riverside Research Institute, New York, NY 10036 USA.

P. M. Goggans is with the Department of Electrical Engineering, University of Mississippi, University, MS 38677 USA.

Publisher Item Identifier S 0018-926X(99)02207-3.

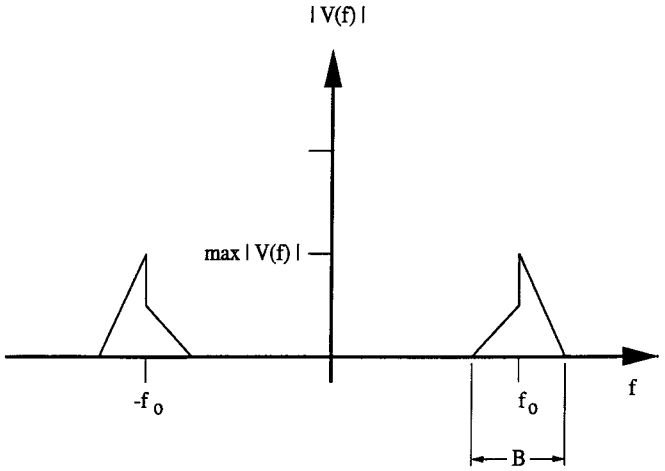

Fig. 1. The frequency-domain spectrum of the bandpass-limited signal $V(f)$.

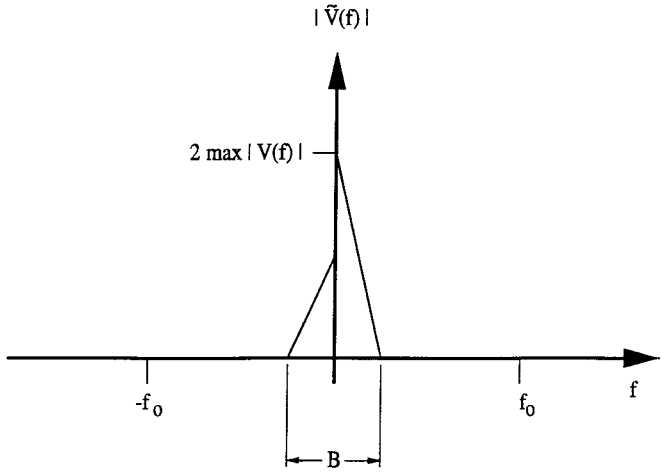

Fig. 2. The frequency-domain spectrum of the lowpass-limited signal $\tilde{V}(f)$.

It is instructional to consider the relationship between $V(f)$ and $\tilde{V}(f)$. Fig. 1 illustrates the Fourier transform $V(f)$ of a real bandpass-limited time function $v(t)$. Because $v(t)$ is real, $V(-f) = V^*(f)$ where the superscript $(\cdot)^*$ denotes the complex conjugate. As a result of this relationship, $v(t)$ can be determined from a knowledge of the positive frequency values of $V(f)$ alone. The transformation makes use of this property by setting the negative frequency portion of $V(f)$ to zero, multiplying by two and then shifting the result to the left by f_0 to yield $\tilde{V}(f)$. If the transformation of $V(f)$ to $\tilde{V}(f)$ is viewed in the graphical way described above, it is clear that $V(f)$ can be obtained from $\tilde{V}(f)$ by reversing the steps above. Fig. 2 illustrates $\tilde{V}(f)$ the Fourier transform of $\tilde{v}(t)$. It is apparent from Fig. 2 that $\tilde{v}(t)$ is low-pass limited. Because in general $\tilde{V}(-f) \neq \tilde{V}^*(f)$, $\tilde{v}(t)$ is in general a complex time function.

III. Complex-Envelope Wave Equations

In electromagnetics, if the sources of the electric and magnetic fields are bandpass-limited, all of the fields resulting from the sources are also bandpass-limited (for linear time-invariant medium). As a result we can write the time and space dependent electric field as

$$\mathbf{E}(\mathbf{r}, t) = \Re\left\{\tilde{\mathbf{E}}(\mathbf{r}, t)\, \exp(j2\pi f_0 t)\right\} \tag{10}$$

where the LPL complex-envelope representation of $\mathbf{E}(\mathbf{r}, t)$ is

$$\tilde{\mathbf{E}}(\mathbf{r}, t) = \mathbf{E_p}(\mathbf{r}, t) + j\mathbf{E_q}(\mathbf{r}, t). \tag{11}$$

In the expressions above, the position vector $\mathbf{r}$ identifies the field point. The real vector functions $\mathbf{E_p}(\mathbf{r}, t)$ and $\mathbf{E_q}(\mathbf{r}, t)$ are the in-phase and quadrature parts of $\mathbf{E}(\mathbf{r}, t)$. Vector quantities are printed in boldface. If the system were also spatially bandpass-limited, a similar transformation could be used to remove the high spatial-frequency variation. However, the spatial-frequency content is dependent on the geometry of the electromagnetic system. Hence, electromagnetic systems are not generally spatially BPL.

The standard real-valued low-pass-limited (base-band) wave equation for linear isotropic time-invariant medium is as follows:

$$\begin{aligned}
&-\nabla^2\mathbf{E} + \left[q\nabla\left(\frac{1}{\varepsilon}\right) + \frac{1}{\varepsilon}\nabla q\right] \\
&\quad - \left[(\mathbf{E}\cdot\nabla\varepsilon)\nabla\left(\frac{1}{\varepsilon}\right) + \left(\frac{1}{\varepsilon}\right)\nabla(\mathbf{E}\cdot\nabla\varepsilon)\right] \\
&\quad + \nabla\times\mathbf{M_i} + \left[\nabla\mu\times\left(\frac{-\nabla\times\mathbf{E} - \mathbf{M_i}}{\mu}\right)\right] \\
&\quad + \mu\dot{\mathbf{J}}_\mathbf{i} + \mu\sigma\dot{\mathbf{E}} + \mu\varepsilon\ddot{\mathbf{E}} = 0
\end{aligned} \tag{12}$$

where μ, ε, and σ are the spatially dependent permeability, permittivity, and conductivity of the medium and where $\mathbf{J_i}$, $\mathbf{M_i}$, and q are the impressed electric current, the impressed magnetic source current and the total electric charge. In (12), a dot above a time function denotes the first partial derivative with respect to time of the function. Similarly, a double dot above a time function denotes the second partial derivative with respect to time of the function.

Using the complex envelope representation of time functions given in (10) and (11), a new complex-valued bandpass-limited form of the vector wave equation

$$\begin{aligned}
&-\nabla^2\tilde{\mathbf{E}} + \left[\tilde{q}\nabla\left(\frac{1}{\varepsilon}\right) + \frac{1}{\varepsilon}\nabla\tilde{q}\right] \\
&\quad - \left[\left(\tilde{\mathbf{E}}\cdot\nabla\varepsilon\right)\nabla\left(\frac{1}{\varepsilon}\right) + \left(\frac{1}{\varepsilon}\right)\nabla\left(\tilde{\mathbf{E}}\cdot\nabla\varepsilon\right)\right] \\
&\quad + \nabla\times\tilde{\mathbf{M}}_\mathbf{i} + \left[\nabla\mu\times\left(\frac{-\nabla\times\tilde{\mathbf{E}} - \tilde{\mathbf{M}}_\mathbf{i}}{\mu}\right)\right] \\
&\quad + \mu\left[\dot{\tilde{\mathbf{J}}}_\mathbf{i} + j2\pi f_0\tilde{\mathbf{J}}\right] + \mu\sigma\left[\dot{\tilde{\mathbf{E}}} + j2\pi f_0\tilde{\mathbf{E}}\right] \\
&\quad + \mu\varepsilon\left[\ddot{\tilde{\mathbf{E}}} + j4\pi f_0\dot{\tilde{\mathbf{E}}} - (2\pi f_0)^2\tilde{\mathbf{E}}\right] = 0.
\end{aligned} \tag{13}$$

can be derived from (12).

In (13), all of the low-pass-limited time functions in (12) are replaced with their complex-envelope representations. We refer to (13) as the complex-envelope vector wave equation. Rewriting (13) for the case where the impressed magnetic current and the conductivity are zero and the permeability is

constant yields the following equation:

$$-\nabla^2\tilde{\mathbf{E}}+\left[\tilde{q}\nabla\left(\frac{1}{\varepsilon}\right)+\frac{1}{\varepsilon}\nabla\tilde{q}\right] -\left[\left(\tilde{\mathbf{E}}\cdot\nabla\varepsilon\right)\nabla\left(\frac{1}{\varepsilon}\right)+\left(\frac{1}{\varepsilon}\right)\nabla\left(\tilde{\mathbf{E}}\cdot\nabla\varepsilon\right)\right] +\mu\left[\dot{\tilde{\mathbf{J}}}_{\mathbf{i}}+j2\pi f_0\tilde{\mathbf{J}}\right]+\mu\varepsilon\left[\ddot{\tilde{\mathbf{E}}}+j4\pi f_0\dot{\tilde{\mathbf{E}}}-(2\pi f_0)^2\tilde{\mathbf{E}}\right]=0. \tag{14}$$

IV. Finite-Difference Time-Domain Formulation

In this paper, we consider a FDTD solution of the complex-envelope representation of the wave equation [4]. The initial work to develop a numerical method for the solution of the complex-envelope wave equation was done using one-dimensional (1-D) geometries [5]. A 1-D version of the standard wave equation (where $q=0$, $\mathbf{M_i}=0$, and μ is constant) can be obtained from (12) by assuming a solution for the electric field that has the single Cartesian vector direction $\hat{\mathbf{z}}$ and is a function of a single spatial coordinate x. This results in the following differential equation:

$$\ddot{E}_z(x,t)-c^2\frac{\partial^2}{\partial x^2}E_z(x,t)=-\mu c^2\dot{J}_z(x,t). \tag{15}$$

Converting (15) to the complex-envelope representation yields

$$\ddot{\tilde{E}}_z(x,t)+j4\pi f_0\dot{\tilde{E}}_z(x,t)-(2\pi f_0)^2\tilde{E}_z(x,t) -c^2\frac{\partial^2}{\partial x^2}\tilde{E}_z(x,t) =-\mu c^2\left[j2\pi f_0\tilde{J}_z(x,t)+\dot{\tilde{J}}_z(x,t)\right]. \tag{16}$$

It is interesting to note that (16) is very similar to the telegraph equation given in [6].

There are many differencing schemes that can be used to approximate (15) and (16). In addition to possessing some specified level of accuracy, the scheme must also be numerically stable. Some schemes will be unconditionally stable, some will be unstable, and some will be conditionally stable.

An explicit second order differencing scheme that approximates (15) is [7]

$$E_z^{n+1}(i)=2[1-\alpha^2]E_z^n(i)+\alpha^2[E_z^n(i-1)+E_z^n(i+1)] -E_z^{n-1}(i) \tag{17}$$

where the Courant–Friedrichs–Lewy (CFL) number [8] is denoted by α and

$$\alpha=c\Delta t/\Delta x. \tag{18}$$

In the equations above, the superscript on E indicates that E is evaluated at an integer multiple of the time step (that is at $t=n\Delta t$ where Δt is the time step). Similarly, the argument of E indicates that E is evaluated at an integer multiple of the spatial step (that is at $x=i\Delta x$ where Δx is the spatial step). This difference scheme is conditionally stable ($\alpha^2\le 1$).

After considerable experimentation, we discovered that (16) can be approximated by the following second-order Crank–Nicolson scheme:

$$-\frac{\alpha^2}{2}\tilde{E}_z^{n+1}(i-1)+[1+(\alpha^2-2\pi^2f_0^2\Delta t^2)+j2\pi f_0\Delta t] \times\tilde{E}_z^{n+1}(i)-\frac{\alpha^2}{2}\tilde{E}_z^{n+1}(i+1) =\frac{\alpha^2}{2}\tilde{E}_z^{n-1}(i-1)-[1+(\alpha^2-2\pi^2f_0^2\Delta t^2)-j2\pi f_0\Delta t] \times\tilde{E}_z^{n-1}(i)+\frac{\alpha^2}{2}\tilde{E}_z^{n-1}(i+1)+2\tilde{E}_z^n(i)+\frac{\Delta t^2\mu c^2}{2} \times\left\{\left[j2\pi f_0\tilde{J}_z^{n+1}(i)+\dot{\tilde{J}}_z^{n+1}(i)\right] +\left[j2\pi f_0\tilde{J}_z^{n-1}(i)+\dot{\tilde{J}}_z^{n-1}(i)\right]\right\}. \tag{19}$$

Crank–Nicolson schemes are often used in the numerical solution of parabolic partial differential equations. A discussion on the use of this type of differencing scheme in the numerical solution of the heat equation can be found in [7] and [9].

For initial-value problems whose finite-difference schemes have constant coefficients, the von Neumann stability condition [7], [10], [11] provides a necessary test of numerical stability. If the scheme is also Hermitian as it is here, the von Neumann stability condition is also a sufficient test of numerical stability [7]. To test (19) for numerical stability, consider a homogeneous source-free region as the domain of interest and assume an initial electric field distribution

$$\tilde{E}_z^0(i)=e^{j\beta i\Delta_x} \tag{20}$$

where β is a real-valued wave number. Now substitute an assumed solution

$$\tilde{E}_z^n(i)=e^{\gamma n\Delta_t}e^{j\beta i\Delta_x} \tag{21}$$

into (19). Doing so yields

$$\left[-\alpha^2\cos(\beta\Delta_x)+1+\alpha^2-\frac{\omega_0^2\Delta_t^2}{2}+j\omega_0\Delta_t\right]e^{\gamma\Delta_t} =2+\left[\alpha^2\cos(\beta\Delta_x)-1-\alpha^2+\frac{\omega_0^2\Delta_t^2}{2}+j\omega_0\Delta_t\right]e^{-\gamma\Delta_t}. \tag{22}$$

If (19) is a numerically stable FD scheme, the von Neumann condition requires that the amplification factor, which is the magnitude of the roots of (22), must always be less than (implies that the scheme is dissipative), or equal to one.

After rewriting (22) in a simpler form

$$ae^{\gamma\Delta_t}+be^{0\gamma\Delta_t}+a^*e^{-\gamma\Delta_t}=0 \tag{23}$$

where

$$a=2+\alpha^2 4\sin(\beta\Delta_x/2)-\omega_0^2\Delta_t^2+j2\omega_0\Delta_t$$
$$b=-4$$

and a^* is the complex conjugate of a, (22) becomes easily recognizable as quadratic in $e^{\gamma\Delta_t}$. Therefore, the roots of (23) are

$$r_\pm=\frac{-b\pm\sqrt{b^2-4aa^*}}{2a} =\frac{-b\pm\sqrt{b^2-4|a|^2}}{2a}. \tag{24}$$

While $|r_{\pm}| \leq 1$ has not been analytically proven for any range of center frequency, frequency bandwidth, time step, and spatial step; numerical computations have shown that $|r_{\pm}| = 1$ for a wide range of center frequency, frequency bandwidth, time step, and spatial step. Furthermore, the amplification factor $|r_{\pm}| = 1$ for every parameter combination tested. This also indicates that this method does not suffer from the numerical dispersion that is inherent in any multidimensional or multigridded explicit finite-difference scheme.

Implicit (Crank–Nicolson) finite-difference solutions can be written in the following matrix form:

$$\overline{\overline{\mathbf{A}}}\mathbf{E}^{n+1} = \overline{\overline{\mathbf{B}}}\mathbf{E}^{n-1} + 2\mathbf{E}^{\mathbf{n}} + \frac{\mathbf{S}^{n+1} + \mathbf{S}^{n-1}}{2} \tag{25}$$

where $\overline{\overline{\mathbf{A}}}$ and $\overline{\overline{\mathbf{B}}}$ are constant, symmetric, and banded (tridiagonal in the 1-D case) matrices, and where $\mathbf{E}^n$ is a column vector made up of the values of $\mathbf{E}$ at all the spatial nodes at the time $n\Delta t$. Similarly, $\mathbf{S}^n$ is a column vector made up of source-related terms at all the spatial nodes at the time $n\Delta t$. Equation (25) is used to determine $\mathbf{E}$ at all of the spatial nodes at time $(n+1)\Delta t$ using the previously determined values of $\mathbf{E}$ at all spatial nodes for times $(n-1)\Delta t$ and $n\Delta t$. Because $\overline{\overline{\mathbf{A}}}$ and $\overline{\overline{\mathbf{B}}}$ are constant and banded (tridiagonal in the 1-D case) the computational burden of solving (25) is relatively small compared to obtaining a solution of (25) if $\overline{\overline{\mathbf{A}}}$ and $\overline{\overline{\mathbf{B}}}$ were dense matrices.

Although the numerical solution of the standard wave equation and complex-envelope formulation of the wave equation can both be obtained using (25), the required time step for the numerical solution of the two different wave equations are very different. For both equations, the selection of the time step is based on the sampling theorem requirements. For the standard wave equation (SWE)

$$\Delta t_{\mathrm{SWE}} = \frac{1}{N f_{\max}} = \frac{1}{N(f_0 + B/2)} \tag{26}$$

where N is the number of samples per period. The sampling theorem states that $N > 2$, however, numerical solutions usually require $N \sim 20$. For the complex-envelope wave equation (CEWE)

$$\Delta t_{\mathrm{CEWE}} = \frac{1}{N(B/2)}. \tag{27}$$

If in the solution of both wave equations N is the same then

$$\Delta t_{\mathrm{CEWE}} = \left[\frac{200}{\%_B} + 1\right]\Delta t_{\mathrm{SWE}} \tag{28}$$

where the percent bandwidth

$$\%_B = 100\,\frac{B}{f_0}. \tag{29}$$

For problems with small percent bandwidth sources, the time step for the complex-envelope wave equation can be several orders of magnitude greater than the time step for the standard wave equation. As a result, the total number of time steps required to obtain a solution to some maximum time using the complex-envelope wave equation can be several orders of magnitude less than that required using the standard wave equation. This and an amplification factor of one are the principle advantages of the complex-envelope formulation. Some of the time-step advantage is lost when the complex-envelope formulation is compared to the standard explicit FDTD method because of the additional calculations that must be performed at each time step in the complex-envelope formulation.

The comparison of the relative time step required in the standard wave- and the complex-envelope wave-equation solutions assumes that choosing N to be the same in both formulations results in similar accuracy. Our initial results confirm this. A fair comparisons between implicit and explicit methods is difficult because for explicit methods, the spatial sampling rate and the time sampling rate are not independent and requirements for spatial sampling often force N to be much larger than is needed for an implicit solution method. Additionally, numerical dispersion decreases the accuracy of multidimensional and multigridded explicit finite-difference schemes. However, one can conservatively state that in all cases

$$\Delta t_{\mathrm{CEWE}} \geq \left[\frac{200}{\%_B} + 1\right]\Delta t_{\mathrm{SWE}}. \tag{30}$$

V. Analytic Solution of the Complex Wave Equation

The solution of the 1-D LPL wave equation for a z-directed surface current J_{sz} at $x = x_o$ in an unbounded homogeneous region is as follows [12]:

$$E_z(x,t) = -\frac{\eta}{2}\left\{J_{sz}\left(t - \frac{x - x_o}{c}\right)u(x - x_o) + J_{sz}\left(t + \frac{x - x_o}{c}\right)u(x_o - x)\right\} \tag{31}$$

where η is the characteristic impedance of the medium and $u(x)$ is the unit step function. It is convenient to use a bandpass-limited time function with a Gaussian envelope for the source current. The source current used here is

$$J_{sz}(t) = -g(t)\left(\frac{2}{\eta}\right)\cos(2\pi f_0 t) \tag{32}$$

where the Gaussian envelope function is

$$g(t) = \exp\left[\frac{-(t - T_0)^2}{2\sigma^2}\right]. \tag{33}$$

In (32), $J_{sz}(t)$ is scaled so that the peak value of $E_z(x, t)$ is one. Note that the Gaussian-shaped envelope is a low-pass limited time function with bandwidth $B = 4/\pi\sigma$. For reasons related to the numerical solution of the wave equation, the time delay is set as $T_o = 4\sigma\sqrt{2}$ so that $g(0)$ is on the order of 10^{-7}. Substituting (32) into (31) gives

$$E_z(x,t) = g\left(t - \frac{x - x_o}{c}\right)\cos\left(2\pi f_0\left[t - \frac{x - x_o}{c}\right]\right) \times u(x - x_o) + g\left(t + \frac{x - x_o}{c}\right) \times \cos\left(2\pi f_0\left[t + \frac{x - x_o}{c}\right]\right)u(x_o - x). \tag{34}$$

Rewriting the cosine terms in (34) as the real part of complex exponential terms and then manipulating the result to obtain the form of (10) yields

$$\tilde{E}_z(x,\,t) = g\left(t - \frac{x-x_o}{c}\right)\exp(-j2\pi f_0(x-x_o)/c) \times u(x-x_o) + g\left(t + \frac{x-x_o}{c}\right) \times \exp(j2\pi f_0(x-x_o)/c)u(x_o-x). \quad (35)$$

Equation (35) is the solution of the 1-D complex-envelope wave equation for a z directed complex-envelope surface current $\tilde{J}_{sz}$ at $x = x_o$ in an unbounded homogeneous region where

$$\tilde{J}_{sz}(t) = -g(t)\left(\frac{2}{\eta}\right). \quad (36)$$

A 1-D cavity with perfect electric conducting (PEC) walls and a plane wave source centered between the walls is used as an example problem in the following section. The PEC walls are at $x = -L/2$ and $x = L/2$ and the source is located at $x = x_o = 0$. Using image theory and (35), the analytic solution of the complex envelope wave equation can be determined. For the plane wave source current of (36), the solution for $\tilde{E}(x,\,t)$ between the cavity walls is

$$\tilde{E}_z(x,\,t) = \sum_{n=0}^{\infty}(-1)^n\left[\tilde{E}_z^L(x,\,t) + \tilde{E}_z^R(x,\,t)\right] \quad (37)$$

where

$$\tilde{E}_z^L(x,\,t) = u(nL+x)g\left(t - \frac{x+nL}{c}\right) \times \exp(-j2\pi f_0(x+nL)/c) \quad (38)$$

and

$$\tilde{E}_z^R(x,\,t) = u(nL-x)g\left(t + \frac{x-nL}{c}\right) \times \exp(j2\pi f_0(x-nL)/c) \quad (39)$$

are the fields to the left and right of the cavity due to the source and its images.

VI. Example Results

A 1-D free-space filled cavity with perfect electric conducting (PEC) walls and a plane wave source centered between the walls is used as an example problem. The PEC walls are at $x = -25\lambda_0$ and $x = 25\lambda_0$ where $\lambda_0 = c/f_0$. The plane wave source is simulated numerically by applying the impressed current at the single spatial node corresponding to the position $x = 0$. In the standard wave-equation solution, the impressed electric current is given by (32). In the complex-envelope wave equation, the impressed current is the complex-envelope representation of $J_{sz}(x_0,\,t)$ as given in (36).

The following example results have been computed with (19), a center frequency, $f_0 = 10$ MHz and a bandwidth, $B = 4$ MHz. The continuous signals were sampled spatially

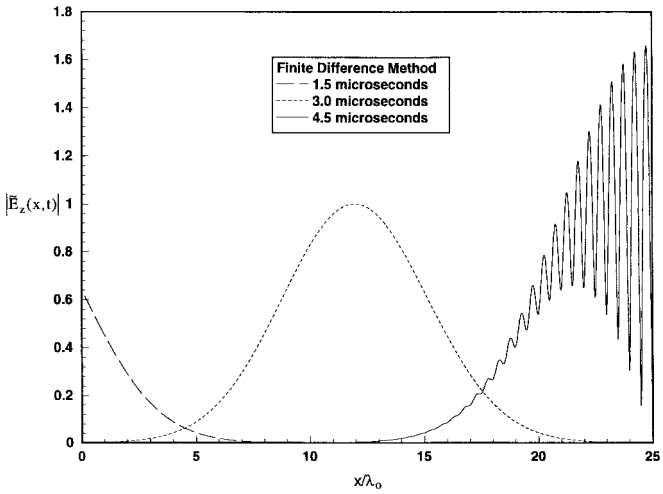

Fig. 3. The BPL FDTD solution of the 1-D cavity problem.

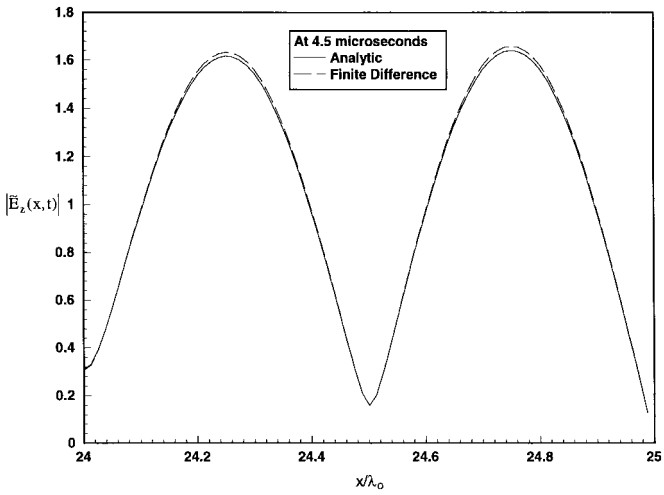

Fig. 4. Comparison of the BPL FDTD and analytic solutions at 4.5 μs.

$(N = 66.\overline{6})$ and temporally $(N = 40)$. Note that the complex-envelope formulation is not particularly computationally advantageous for this combination of parameters $(\Delta t_{\mathrm{CEWE}} = 6\Delta t_{\mathrm{SWE}})$, however, these values were used so that the spatial oscillations of the solution can be displayed clearly.

Fig. 3 illustrates the FDTD solution of the 1-D scalar complex-envelope wave equation. Because the cavity is symmetric, the field distribution is only given for one half of the cavity. At 1.5 and 3.0 μs the traveling waves have not yet propagated to the walls of the cavity. The rapid variation in the field strength at 4.5 μs is due to the backward traveling (reflected) wave interfering with the forward traveling wave. Given that Fig. 3 is a plot of the magnitude of the envelope of a radio frequency (RF) signal, this rapid variation is expected.

A comparison of the analytic and BPL FDTD solutions is shown in Fig. 4. The field distributions for 4.5 μs at the edge of the cavity are plotted. The largest error is observed in this region of the cavity. The BPL FDTD solution is in excellent agreement with the analytic solution. The maximum observed error in the complex-valued solution is less than 2%.

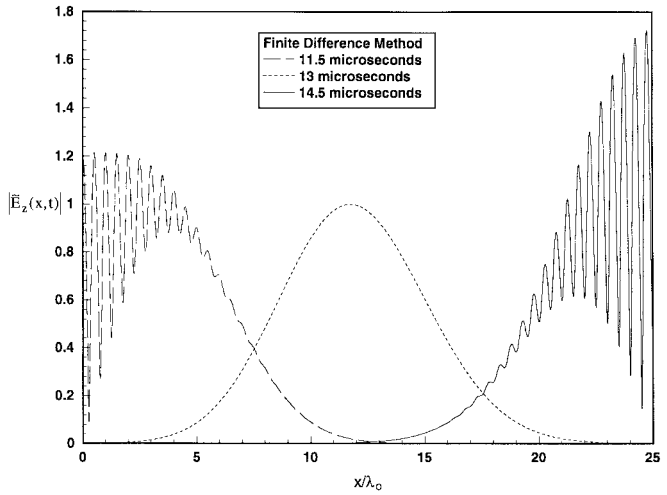

Fig. 5. The BPL FDTD solution of the 1-D cavity problem..

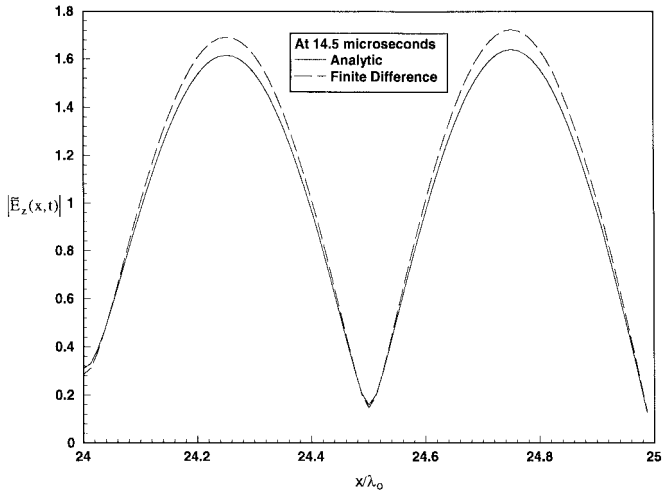

Fig. 6. Comparison of the BPL FDTD and analytic solutions at 14.5 μs.

The field distributions at later times are illustrated in Figs. 5 and 6. In Fig. 5, the field distribution at 14.5 μs has propagated more than 125 m and is in the process of completing its third reflection. A comparison with the analytic solution at 14.5 μs is shown in Fig. 6. While the error in the BPL FDTD solution has increased, it is still less than 5%. This cumulative error is due to the finite-difference approximations of the temporal- and spatial-derivatives.

A dielectric interface is used as a second example problem. To the left $(x/\lambda_0 < 12)$ of the interface is free space. To the right $(x/\lambda_0 \geq 12)$ the relative permittivity is two. Note that the spatial dimension of the 1-D cavity was extended so that during the times of interest, there would be no reflection from the PEC walls. The frequency and sampling parameters remain the same as in the first example. Fig. 7 illustrates the BPL FDTD computed field distributions for various times in the region of the interface. At 1.5 μs, the field has not yet propagated to the interface. The field is in the process of being transmitted through and reflected from the interface at 3.0 μs. At 4.5 μs, the reflected field is propagating to the left, while the transmitted field is propagating to the right. The reflection and transmission coefficients are within 0.1% of the analytic values.

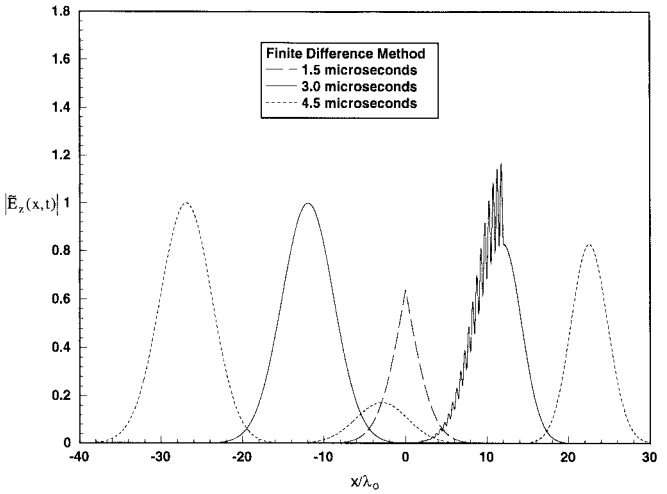

Fig. 7. The BPL FDTD solution of a region with a dielectric interface.

VII. Conclusions

Using the complex-envelope representation of bandpass-limited signals, a new bandpass-limited formulation of the vector wave equation was formulated and presented here. A new bandpass-limited FDTD scheme that solves the bandpass-limited vector wave equation has been developed and presented. An amplification factor of one and the ability to set the time-step size based solely on the bandwidth of the system are the principle advantages of this new method. For narrow-band (small percent bandwidth) systems, the time step can be several orders of magnitude larger than the time step in conventional FDTD methods.

Results that illustrate the accuracy of this new method were presented. While these results were for a 1-D cavity, the formulation is valid in two and three dimensions as well. Preliminary two-dimensional (2-D) results indicate that the method is numerically stable and accurate. The authors are currently working on a comprehensive error analysis of the 1-D formulation, application of an absorbing boundary condition, and the verification of 2-D results.

References

[1] S. Haykin, *Communication Systems*, 2nd ed. New York: Wiley, 1983.
[2] P. M. Goggans and J. D. Pursel, "Radar time- and frequency-domain received signals for realistic antennas and scatterers," in *12th Annu. Rev. Progress Appl. Computat. Electromagn.*, Monterey, CA, 1996, vol. 12.
[3] A. Papoulis, *The Fourier Integral and Its Applications.* New York: McGraw-Hill, 1962.
[4] J. D. Pursel, "A finite-difference time-domain solution of the second-order bandpass-limited electromagnetic wave equation," Ph.D. dissertation, Univ. Mississippi, 1998.
[5] P. M. Goggans and J. D. Pursel, "Using time-domain complex-envelope representations of band-pass-limited signals in the finite-difference solution of the wave equation," in *North Amer. Radio Sci. Meet.*, Montreal, Canada, July 1997, p. 128.
[6] R. Courant and D. Hilbert, *Methods of Mathematical Physics— Vol. II.* New York: Intersci., 1962.
[7] E. Isaacson and H. B. Keller, *Analysis of Numerical Methods.* New York: Wiley, 1966.
[8] R. Courant, K. Friedrichs, and H. Lewy, "On the partial difference equations of mathematical physics," *IBM J. Res. Develop.*, vol. 11, no. 1, pp. 215–234, 1967; "Uber die partiellen differenzengleichungen der mathematischen physik," *Math. Ann.*, vol. 100, pp. 32–74, 1928 (Engl. transl.).

[9] B. Gustafsson, H. Kreiss, and J. Oliger, *Time Dependent Problems and Difference Methods.* New York: Wiley, 1995.
[10] P. D. Lax, "Hyperbolic difference equations: A review of the Courant–Friedrichs–Lewy paper in the light of recent developments," *IBM J. Res. Development*, vol. 11, no. 1, pp. 235–238, 1967.
[11] R. D. Richtmyer and K. W. Morton, *Difference Methods for Initial-Value Problems*, 2nd ed. New York: Wiley, 1967.
[12] I. V. Lindell, *Methods for Electromagnetic Field Analysis.* Oxford, U.K.: Oxford Univ. Press, 1992.

J. D. Pursel (S'90–M'99) was born in Bakersfield, CA, on July 3, 1969. He received the B.S.E.E. degree from the California State University at Fresno, in 1993, and the M.S. and Ph.D. degrees in engineering science from the University of Mississippi, University, MS, in 1995 and 1998, respectively.

He served as a Graduate Instructor and Research Assistant in the Department of Electrical Engineering at the University of Mississippi under a Graduate Assistance Areas of National Need Fellowship. In May 1998 he joined the Electromagnetics Directorate of the Riverside Research Institute, New York, NY. His current research interests are optimization, finite-difference time-domain methods, and the use of high-performance computing in the solution of electromagnetics problems.

Dr. Pursel is a member of the Eta Kappa Nu and Tau Beta Pi honor Societies, the Sigma Xi Society of scientific research, the Antennas and Propagation, Electromagnetic Compatibility, and Microwave Theory and Techniques Societies of IEEE, and the Society of Industrial and Applied Mathematics.

P. M. Goggans (S'78–M'89) was born in Opelika, AL, on September 13, 1954. He received the B.S. and M.S. degrees in electrical engineering in 1976 and 1978, respectively and the Ph.D. degree in 1990, all from Auburn University, Auburn, AL.

From 1979 to 1985, he was employed by Sandia National Laboratories, Albuquerque, NM, in the Radar Signal Analysis Division. From 1985 to 1990 he was with Auburn University as an Instructor while working toward the Ph.D. degree. In 1990 he was appointed Assistant Professor in the Department of Electrical Engineering at the University of Mississippi, Oxford, MS. In 1994 he was promoted to Associate Professor. His research interests include computational electromagnetics methods based on integral equation and differential equation formulations, the application of signal processing techniques to the development of computational solutions for electromagnetic applications, and the electromagnetic and signal processing aspects of radar systems.

Dr. Goggans is a member of Eta Kappa Nu, Phi Kappa Phi, the Audio Engineering Society, and the IEEE Antennas and Propagation, Microwave Theory and Techniques, Electromagnetic Compatibility, and Education Societies.